tvst

Retina

Establishing Fully-Automated Fundus-Controlled Dark Adaptometry: A Validation and Retest-Reliability Study

Jeannine M. Oertli [1], Kristina Pfau [1], Hendrik P. N. Scholl [1,2], Brett G. Jeffrey [3], and Maximilian Pfau [1,2]

[1] Department of Ophthalmology, University Hospital Basel, Basel, Switzerland
[2] Institute of Molecular and Clinical Ophthalmology Basel, Basel, Switzerland
[3] Ophthalmic Genetics and Visual Function Branch, National Eye Institute, National Institutes of Health, Bethesda, MD, USA

Correspondence: Maximilian Pfau, Institute of Molecular and Clinical Ophthalmology Basel, Mittlere Strasse 91, Basel CH-4031, Switzerland. e-mail: maximilian.pfau@iob.ch

Received: August 9, 2023
Accepted: November 14, 2023
Published: December 19, 2023

Keywords: dark adaptation; microperimetry; visual psychophysics

Citation: Oertli JM, Pfau K, Scholl HPN, Jeffrey BG, Pfau M. Establishing fully-automated fundus-controlled dark adaptometry: A validation and retest-reliability study. Transl Vis Sci Technol. 2023;12(12):18, https://doi.org/10.1167/tvst.12.12.18

Purpose: The purpose of this study was to establish and validate a novel fundus-controlled dark-adaptometry method.

Methods: We developed a custom dark-adaptometry software for the S-MAIA device using the open-perimetry-interface. In the validation-substudy, participants underwent dark-adaptometry testing with a comparator device (MonCvONE, 59% rhodopsin bleach, cyan and red stimuli centered at 2 degrees, 4 degrees, and 6 degrees eccentricity). Following a brief break (approximately 5 minutes), the participants were bleached again and underwent dark-adaptometry testing with the S-MAIA device (same loci). In the retest reliability-substudy, participants were tested twice with the S-MAIA device (same loci as above). Nonlinear curve fitting was applied to extract dark-adaptation curve parameters. Validity and repeatability were summarized in terms of the mean bias and 95% limits of agreement (LoAs).

Results: In the validation-substudy ($N = 20$ participants, median age interquartile range [IQR] 31.5 years [IQR = 25.8, 62.0]), measures of rod-mediated dark-adaptation showed little to no between method differences for the cone-rod-break-time (bias 95% confidence interval [95% CI] of +0.1 minutes [95% CI = −0.6 to 0.8]), rod-intercept-time (−0.23 minutes [95% CI = −1.38 to 0.93]), and S2 slope (−0.01 LogUnits/minutes [95% CI = −0.02 to −0.01]). In the retest reliability-substudy ($N = 10$ participants, 32.0 years [95% CI = 27.0, 57.5]), the corresponding LoAs were (cone-rod-break-time) −3.94 to 2.78 minutes, (rod-intercept-time) −4.55 to 3.11 minutes, and (S2 slope [rate-limited component of rod recovery]) −0.03 to 0.03 LogUnits/minutes. The LoAs for the steady-state cone and rod thresholds were −0.28 to 0.33 LogUnits and −0.34 to 0.28 LogUnits.

Conclusions: The devised fundus-controlled dark-adaptometry method yields valid and reliable results.

Translational Relevance: Fundus-controlled dark-adaptometry solves the critical need for localized testing of the visual cycle and retinoid transfer in eyes with unstable fixation.

Introduction

Early slowing of rod photoreceptor-mediated dark adaptation is characteristic for systemic vitamin A deficiency,[1] inherited retinal diseases (IRDs) due to Bruch's membrane alterations,[2–6] and enzymatic visual cycle dysfunction,[7,8] as well as for age-related macular degeneration (AMD),[9–12] which constitutes the most common cause of legal blindness in industrialized countries.[13] In these diseases, the ability to dark adapt following bright light exposure is typically impaired before fully dark-adapted rod sensitivity is lost (i.e. dynamic dysfunction preceding steady-state dysfunction).[4,11,14,15]

Today, a plethora of methods are available for evaluating steady-state cone and rod function. Steady-state cone and rod dysfunction can be assessed using full-field electroretinography (retina-wide sum), and in a spatially resolved manner using light- and

dark-adapted two-color perimetry,[16,17] or chromatic pupil campimetry.[18] Recently, dark-adapted two-color microperimetry (i.e. fundus-controlled perimetry) became available, enabling spatially resolved testing of rod function even in patients with unstable fixation.[19–24]

For the testing of dynamic rod dysfunction, less options are available. Devices like the AdaptDx adaptometer (MacuLogix, Harrisburg, PA, USA) or the MonCvONE (Pérenchies, France) are not fundus-controlled (i.e. free-viewing stimulus presentation).[25,26] These free-viewing devices (as opposed to fundus-controlled microperimetry devices) are unsuitable for testing of patients with unstable fixation and assessing small, localized regions of interest in a patient-tailored manner.

To address these shortcomings, using the MP1 device has been proposed for fundus-controlled dark adaptometry.[27,28] However, due to the limited dynamic range of the device, this method necessitated adding optical filters and changing the stimulus size within test runs. Additionally, the workflow was also not fully automated, hindering its application in multicenter therapeutic trials.

Thus, we have now devised a fundus-controlled dark-adaptometry method for evaluating the rod-mediated dark adaptation in patients with unstable fixation using an external bleach followed by threshold testing with a scanning laser ophthalmoscopy (SLO)-based microperimetry device (S-MAIA; Icare/CenterVue S.p.A., Padova, Italy). As a prerequisite to the clinical application, we have evaluated the concurrent validity against the commercially available MonCvONE device, test-retest reliability, and construct validity of the devised method.

Methods

Participants

This study was approved by the ethics committee for Northwestern and Central Switzerland (EKNZ) and adhered to the Declaration of Helsinki. Participants were informed of the study procedures and provided written informed consent before participating.

To be included, participants had to be older than 18 years and have no history of ocular surgery that – according to the investigator's judgment – may affect visual function assessments exceptions: cataract surgery, YAG laser capsulotomy, or laser retinopexy. Participants were initially enrolled in the validation substudy and subsequently in the test-retest reliability substudy. Participants could be enrolled in both substudies. In participants with two eligible eyes, one eye was selected as the study eye at random.

Core Examinations

All participants underwent autorefraction followed by best-corrected visual acuity (BCVA) testing using the qVA protocol Manifold platform (Adaptive Sensory Technology, Lübeck, Germany). After the psychophysical tests (described below), the participants underwent spectral-domain optical coherence tomography imaging (SD-OCT including a macular volume of 30 degrees × 25 degrees with 121 B-scans [automatic real time averaging 25], and the preset Bruch's membrane opening [BMO] scan; Heidelberg Spectralis OCT2; Heidelberg Engineering, Heidelberg, Germany) to exclude any retinal or optic nerve head disease.

Between-Device Validation Substudy

Following pupil dilatation, participants in the validation substudy (enrollment target $N = 20$) underwent dark adaptometry testing with the MonCvONE device (Metrovision, Perenchies, France). The participants were bleached with the pre-set full-field 634 photopic cd/m^2 (946 scotopic cd/m^2) bleach for 5 minutes, corresponding to a 59% rhodopsin bleach.[14,29] Following the bleach, cyan and red Goldmann V-sized stimuli (peak wavelengths of 500 nm and 647 nm, stimulus duration 200 ms) were presented at 2 degrees, 4 degrees, and 6 degrees eccentricity to the fovea.

We selected these loci close to the rod-free zone, given that psychophysical data,[14,26] and histopathologic data,[30] suggest rod dysfunction in close proximity to the fovea could constitute an early marker of AMD.

We tested either along the nasal or temporal horizontal meridian. The laterality (nasal or temporal) was selected randomly. The thresholds were continuously determined for all loci in a single 30-minute test-run using the pre-set "5-up-1-down staircase" strategy. The examiner was allowed to terminate the test earlier if the final rod threshold was reached before 30 minutes.

For the newly devised method, we developed a custom *R* package utilizing the open perimetry interface (OPI) to communicate with the S-MAIA device,[31,32] and *R Shiny* to provide a graphical user interface through a web application.[33] The dark adaptation testing software and a manual are available as an *R* package (https://github.com/maximilianpfau/darkOPI [GNU GPL version 3 license]).

Using the OPI workflow for the S-MAIA device, we first acquired the baseline fundus image and

performed the brief initial fixation exam (approximately 10 seconds). Then, the participant was bleached with the MonCvONE device using the bleach specified above (any Ganzfeld or Maxwellian-view set-up could be used to deliver the bleach instead). After the 5-minute bleach, the participant had to position himself or herself in front of the S-MAIA device again quickly, and the fundus-controlled stimulus presentation started. Again, cyan and red stimuli (peak wavelengths: 505 nm and 627 nm; size: Goldmann III, duration: 200 ms) were presented with 2 degrees, 4 degrees, and 6 degrees eccentricity to the fovea. The laterality (nasal/temporal retina) was matched with the MonCvONE test. A 5-up-1-down staircase strategy was used to obtain each threshold. The tests ran for 30 minutes. The examiner was allowed to terminate the test earlier if the final rod thresholds were reached.

Test-Retest Reliability Substudy

In another 10 participants, we performed dark adaptation measurements with the devised S-MAIA-based method twice to determine the test-retest reliability of the devised method. Again, the stimuli could be presented nasally or temporally along the horizontal meridian, but the position within each participant was identical for both tests. Between the two tests, participants were allowed to rest for up to 10 minutes in the dark room. Participants were offered water and coffee.

Curve Fitting

For dark adaptation curve estimation ("darkest"), we developed a wrapper package in *R* using the *R* package *brms* for nonlinear curve fitting.[34] The software is available at: https://github.com/maximilianpfau/darkest (GNU GPL version 3 license).

For the dark adaptation curves from the MonCvONE, we used a regression formula describing both the cone and rod-mediated dark adaptation (modified from Flynn et al.).[14]

$$Threshold(time) = \begin{cases} CT + (T_0 - CT) * \exp\left(-\frac{time}{tau}\right) \\ \quad + \log_{10}\left(10^{(S2*(time-CRB))} + 10^{(RT-CT)}\right), & \text{if } time > CRB \\ & \wedge\ stimulus = cyan \\ CT + (T_0 - CT) * \exp\left(-\frac{time}{tau}\right), & \text{otherwise} \end{cases} \quad (1)$$

where

$Threshold(time)$ = threshold (LogUnits) at a time (min)
T_0 = initial threshold (LogUnits)
tau = exponential cone recovery time constant (min^{-1})
CT = cone threshold (LogUnits)
CRB = cone-rod break time (min)
$S2$ = S2 slope (LogUnits/min)
RT = final rod threshold (LogUnits)

We applied weakly informative priors for curve fitting that spanned the plausible value range for the curve parameters (Supplementary Table S1).

For the dark adaptation curves from the S-MAIA device, we used a regression formula representing the cone threshold (during the cone plateau) and the rod-mediated dark adaptation phase becuase the first phase was not recorded (due to the time required to move the participant to the S-MAIA device after the bleach).

$$Threshold(time) = \begin{cases} CT + \log_{10}\left(10^{(S2*(time-CRB))} + 10^{(RT-CT)}\right), & \text{if } time > CRB \\ & \wedge\ stimulus = cyan \\ CT, & \text{otherwise} \end{cases} \quad (2)$$

Data from the red stimuli were included in the fitting procedure up to <12 minutes. We excluded later red stimulus data from the curve fitting because eventual rod-meditation of the red stimulus was evident in most participants (cf., Fig. 1).

In addition, we extracted the rod intercept time (RIT) defined as the time to reach a criterion threshold of 1 LogUnit below the cone threshold (i.e. based on our average 6 degrees cone threshold estimates across participants, the criterion thresholds were defined as −5.9 LogUnits for the MonCvOne and −1.4 LogUnits for the S-MAIA device).

To facilitate the comparison of the threshold estimates, we subtracted 4.3 LogUnits from MonCvONE-based measurements accounting for average cone threshold difference at 2 degrees, 4 degrees, and 6 degrees in the dB-scales between the devices.

Statistical Analysis

All statistical analyses were performed in the software environment *R*. The data are available at Zenodo (https://doi.org/10.5281/zenodo.10219425).

BCVA and age were summarized based on their median and interquartile range. Data from participants tested at the temporal or nasal retina were pooled, given the absence of relevant differences (in relation to the retest reliability).

To evaluate the (1) between-method validity and the (2) retest reliability, we used Bland-Atman plots and statistics. For all analyses stratified by eccentricity, we used an intercept-only model to describe the measurement difference in terms of the mean bias with the 95% confidence interval (CI), and the 95% prediction intervals as the limits of agreement. For the joint analysis of the data from the three eccentricities, we fitted

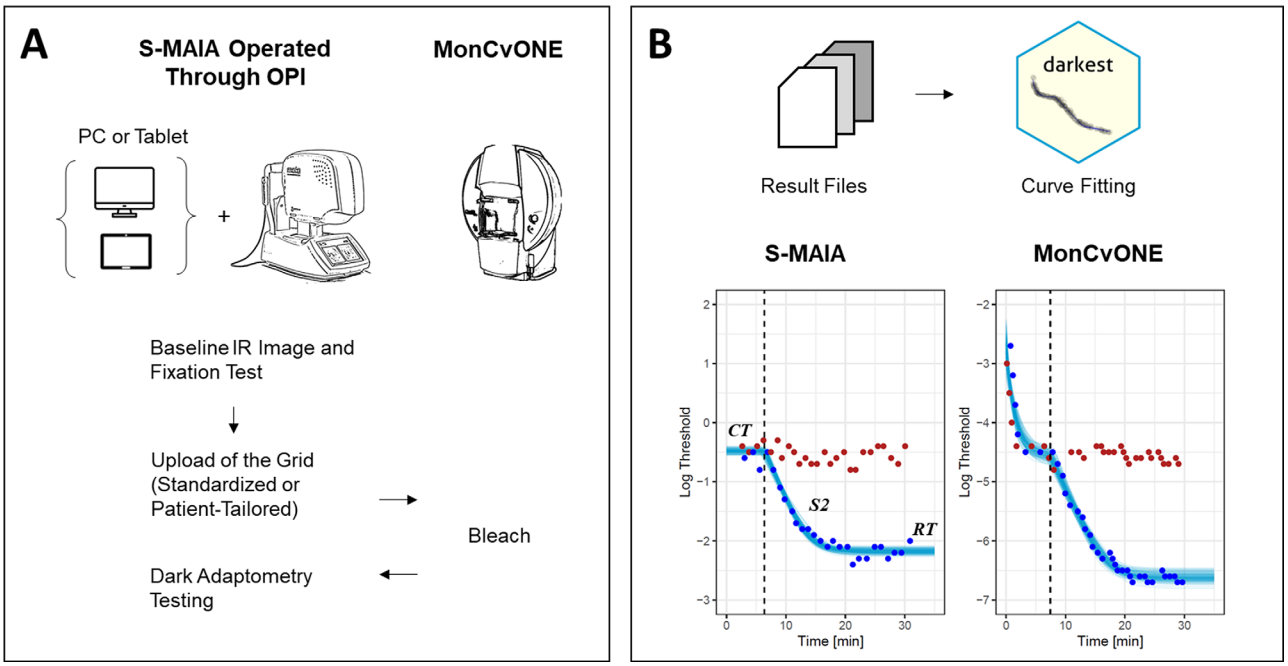

Figure 1. Dark Adaptation with the S-MAIA Device and the MonCvONE Comparator Device. Panel (**A**) shows the workflow for the devised S-MAIA-based fundus-controlled dark adaptometry testing. In brief, participants were positioned in front of the S-MAIA device for a baseline infrared image and a short fixation test. Subsequently, the grid was uploaded to the custom software. Participants were then exposed to a background light that bleached the retina. Once the bleach was finished, the participants quickly returned to the S-MAIA device for threshold testing. Panel (**B**) shows typical dark adaptation curves (at 6 degrees). Of note, the cone adaptation was typically not resolved with the S-MAIA-based testing due to the time required to switch from the MonCvONE device to the S-MAIA device. The *red* and *blue dots* denote the threshold for red and cyan stimuli. The semi-transparent lines show draws from the expectation of the posterior predictive distribution from the Bayesian nonlinear curve fit (i.e. distribution of plausible curve fits conditional on the observed values). The *dashed vertical line* denotes the cone-rod break time. CT, cone threshold; S2, rate-limited slope of the rod adaptation; RT, rod threshold.

an intercept-only mixed model with the participant as a random effect to account for the repeated measures within each participant.

To substantiate the (3) construct validity (based on the established relationship between aging and impaired dark adaptation),[35] we fitted mixed models with the given dark adaptation curve parameters as the dependent variable, and age and eccentricity as the independent variables, and participant as a random effect. We applied linear regression as an approximation given prior data supporting a linear relationship of these parameters with age.[35]

Results

Between-Method Comparison Substudy

A total of 23 participants were enrolled in the validation cohort. Of those, 20 were included in the between-method validation analysis (median age, interquartile range [IQR] 31.5 years [IQR = 25.8, 62.0]; Table 1).

Table 1. Participant Characteristics

	Validation Study ($N = 20$)	Retest Study ($N = 10$)
Best-corrected visual acuity (LogMAR)		
Median [Q1, Q3]	−0.07 [−0.07, −0.07]	−0.07 [−0.07, −0.07]
Age (y)		
Median [Q1, Q3]	31.5 [25.8, 62.0]	32.0 [27.0, 57.5]
Sex		
Female	9 (45.0%)	7 (70.0%)
Male	11 (55.0%)	3 (30.0%)

One participant was excluded from the analysis due to intermediate AMD, evidenced by multimodal imaging at the end of the study visit. Two participants were excluded from the analysis, because the laterality (nasal/temporal retina) was inadvertently flipped between the devices.

The MonCvONE and S-MAIA-based measurements yielded similar estimates for the dynamic measure of dark adaptation (Table 2, Fig. 2). Specifically, there was no significant bias (MonCvONE - S-MAIA [95% CI] = +0.1 minutes [95% CI = −0.6, 0.8])

Table 2. Between-Device Differences in Dark Adaptation Curve Parameters

Parameter	Unit	Bias* [95% CI]	Lower LoA	Upper LoA
Cone rod break time (CRB)	Min	0.1 [−0.6, 0.8]	−3.66	3.86
Rod intercept time (RIT)	Min	−0.23 [−1.38, 0.93]	−6.72	6.26
S2 slope	LogUnits per Min	−0.01 [−0.02, −0.01]	−0.06	0.03
Cone threshold	LogUnits	0.01 [−0.11, 0.13]	−0.62	0.64
Rod threshold	LogUnits	−0.41 [−0.5, −0.32]	−1.02	0.2

LoA, limit of agreement.
*The values represent the MonCvONE minus S-MAIA difference.

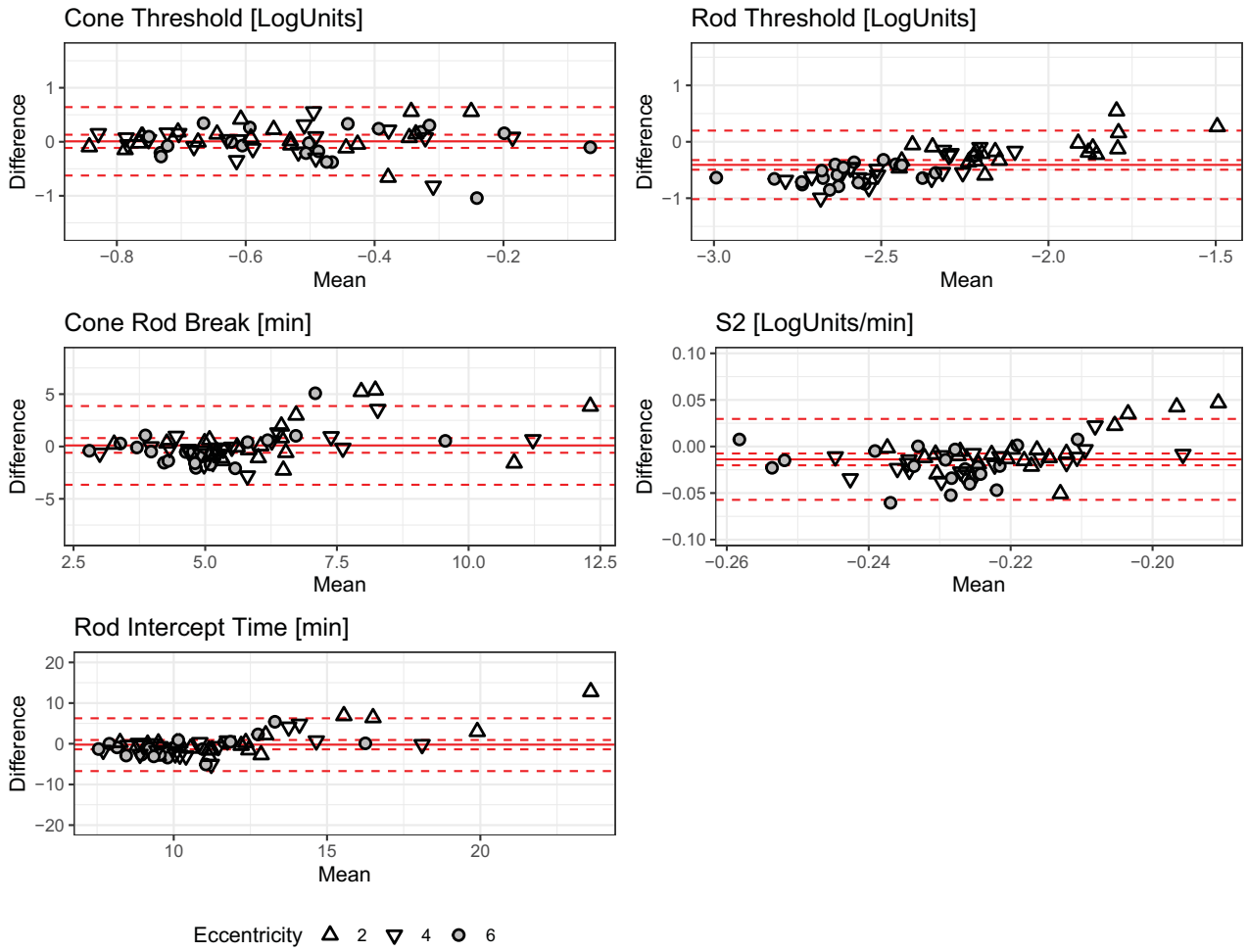

Figure 2. **Between-Method Comparison.** The Bland-Altman (mean-difference) plots show the between-method differences (MonCvONE minus S-MAIA) for the five parameters from the dark adaptation curve fitting. The shape denotes eccentricity (see legend). The *solid red lines* show the mean bias, the *dashed inner lines* show the 95% confidence interval, and the *dashed outer lines* show the 95% prediction intervals (limits of agreement). For the rod threshold (and the S2 slope), there is evidence of a systematic difference. Especially, at 4 degrees and 6 degrees eccentricity, the MonCvONE rod thresholds are slightly lower (cf. Supplementary Table S3).

for the cone-rod break with limits of agreement (LoAs) of −3.66 minutes and 3.86 minutes. Likewise, there was no significant bias for the rod intercept time (bias [95% CI] of −0.23 minutes [95% CI = −1.38 to 0.93]; LoAs of −6.72 minutes and 6.26 minutes).

In contrast, the S2 slope was minimally steeper (i.e. more negative) in MonCvONE-based dark adaptation curves (bias [95% CI] of −0.01 LogUnits/min [95% CI = −0.02 to −0.01], LoAs of −0.06 LogUnits/min to 0.03 LogUnits/min).

Table 3. Test-Retest Reliability of the Dark Adaptation Curve Parameters

Parameter	Unit	Bias* [95% CI]	Lower LoA	Upper LoA
Cone rod break time (CRB)	Min	−0.58 [−1.38, 0.21]	−3.94	2.78
Rod intercept time (RIT)	Min	−0.72 [−1.57, 0.13]	−4.55	3.11
S2 slope	LogUnits per Min	0 [−0.01, 0]	−0.03	0.03
Cone threshold	LogUnits	0.02 [−0.04, 0.09]	−0.28	0.33
Rod threshold	LogUnits	−0.03 [−0.09, 0.03]	−0.34	0.28

LoA, limit of agreement.
*The values represent the first minus second test difference.

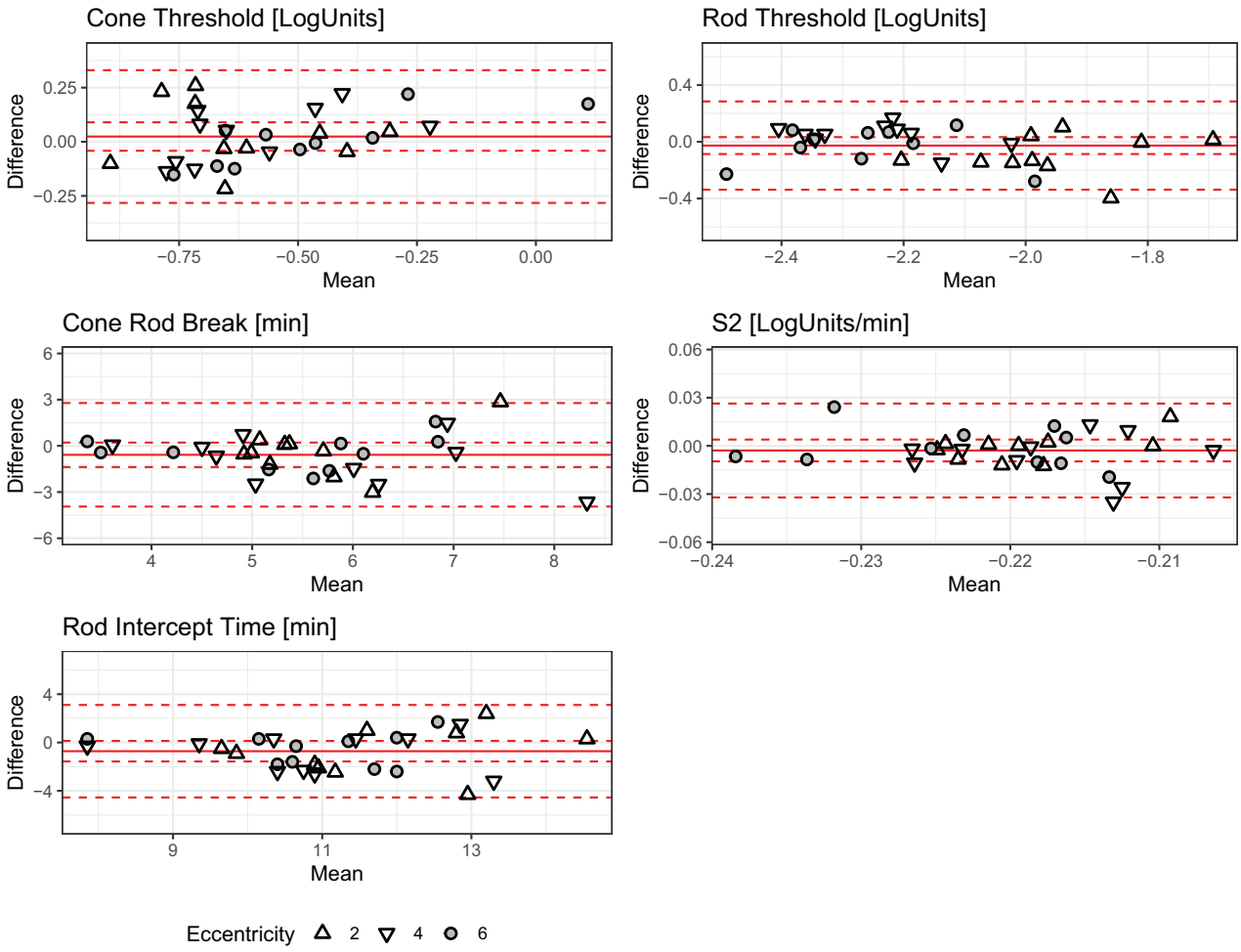

Figure 3. **Test-Retest Reliability.** The Bland-Altman (mean-difference) plots show the test-retest reliability for the five parameters from the dark adaptation curve fitting. The shape denotes eccentricity. The *solid red lines* show the mean bias, the *dashed inner lines* show the 95% confidence interval, and the *dashed outer lines* show the 95% prediction intervals (limits of agreement).

The steady-state threshold parameters showed (after accounting for the instrument-specific dB scales) excellent agreement for the cone threshold with a bias of 0.01 LogUnits [−0.11, 0.13] and LoAs of −0.62 LogUnits and 0.64 LogUnits. The final rod thresholds were significantly lower for the MonCvONE-based measurements with a bias of −0.41 LogUnits [−0.5, −0.32] and LoAs of −1.02 LogUnits and 0.2 LogUnits (cf. Supplementary Table S3).

The estimated curve parameters are shown in Supplementary Table S2. The between-method differences were overall similar across eccentricities (see Supplementary Table S3).

Test-Retest Reliability Substudy

Ten participants were enrolled in the intra-session test-retest reliability cohort (median age [IQR] of 32.0 years [IQR = 27.0, 57.5]; see Table 1).

Overall, the intra-session test-retest reliability estimates showed no significant biases (i.e. no evidence of learning or fatigue effects), and the reliability was similar across all value ranges (Table 3, Fig. 3).

The bias [95% CI] for the cone-rod break was −0.58 minutes [95% CI = −1.38 to 0.21] with LoAs of −3.94 minutes and 2.78 minutes, and for the rod intercept time −0.72 minutes [95% CI = −1.57 to 0.13] with LoAs of −4.55 minutes and 3.11 minutes. The bias for the S2 slope was 0 LogUnits/min [−0.01, 0] with LoAs of −0.03 LogUnits/min and 0.03 LogUnits/min.

For the steady-state threshold parameters, the test-retest reliability was excellent. For the cone threshold, the bias was 0.02 LogUnits [−0.04, 0.09] with LoAs of −0.28 LogUnits and 0.33 LogUnits, for the final rod threshold −0.03 LogUnits [−0.09, 0.03] with LoAs of −0.34 LogUnits and 0.28 LogUnits.

The test-retest reliability was similar across eccentricities (Supplementary Table S4).

Association With Age

All S-MAIA-based data (validity and retest cohorts) from a total of 26 participants were pooled to assess the association of age with the curve parameters. All dark adaptation parameters increased with age, except for the cone threshold and S2 slope (Fig. 4, Supplementary Table S5).

The cone thresholds followed the hill-of-vision with slightly lower thresholds (i.e. better sensitivity) at 2 degrees (intercept estimate of −0.74 LogUnits)

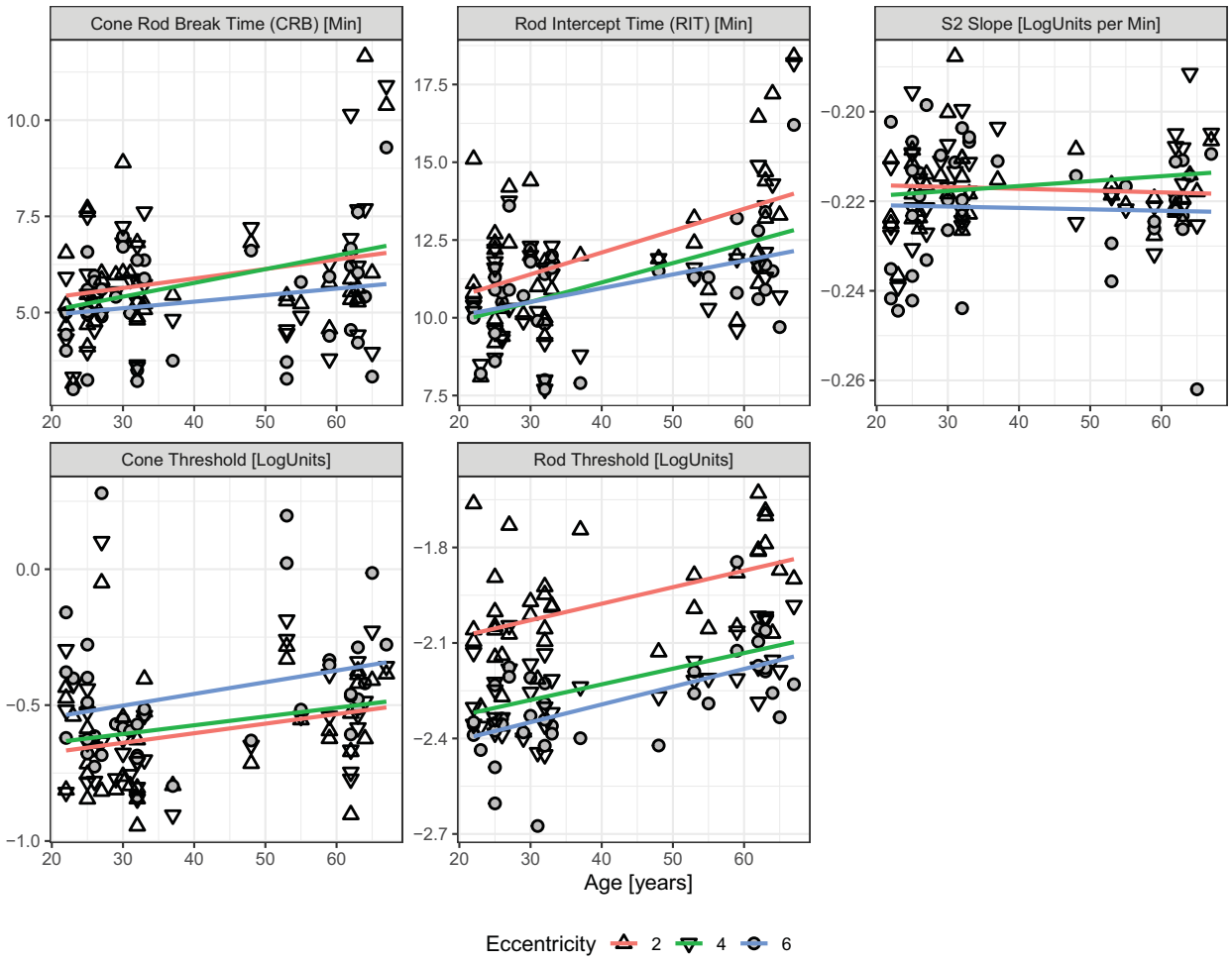

Figure 4. Association of Age with Dark Adaptation Parameters. The panels plot the dark adaptation curve parameters as a function of age. The shape denotes eccentricity. The regression lines are individual linear regression lines fitted for each eccentricity. The changes with age are similar across the three tested locations (i.e. no pronounced interaction effect between age and eccentricity). Please note, we applied linear regression as a first-order approximation (given prior data supporting a linear relationship of these parameters with age).[35]

compared to 4 degrees and 6 degrees (+0.03 LogUnits and +0.14 LogUnits). The association between cone sensitivity and age was not significant (slope estimate [95% CI] 0.04 LogUnits per decade [95% CI = −0.01 to 0.09], $P = 0.133$).

In contrast, the rod threshold decreased with eccentricity (intercept of −2.16 LogUnits; effect estimates of −0.25 LogUnits for 4 degrees, and −0.32 LogUnits for 6 degrees eccentricity). The rod thresholds were elevated in older participants (slope estimate [95% CI]) 0.05 LogUnits per decade [95% CI = 0.02, 0.07], $P < 0.001$). The rod intercept time – as a measure of dynamic function – was associated with age, too (0.61 minutes per decade [95% CI = 0.23, 0.98], $P = 0.002$).

Discussion

Slowing of rod-mediated dark adaptation is among the earliest visual function alterations in AMD,[9–12] and in IRDs due to Bruch's membrane alterations,[2–6] and enzymatic visual cycle dysfunction.[7,8] Previous and ongoing clinical studies focus predominantly on patients with stable fixation and large stimulus testing (Goldmann V or larger).[25,26] The now-devised method offers a fully automated workflow for fundus-controlled dark adaptometry testing for evaluating patients with unstable fixation in a highly localized manner.

Critical advantages of the devised workflow for measuring thresholds during the dark adaptation phase are: (1) fundus tracking to examine patients with unstable fixation, (2) two-color testing to distinguish rod from cone mediation, (3) providing a fully automated software for testing and analysis, and (4) offering flexibility and precision for stimulus placement. Especially in the era of localized treatment (e.g. subretinally delivered gene therapies), this workflow provides the opportunity to test changes in function over time at specific regions of interest in a highly localized manner. Analogously to the previous concept of patient-tailored perimetry,[36–38] the devised workflow will enable researchers to use adaptometry to track leading disease fronts instead of coarse "retina-wide" testing.

Previously, Wadim Bowl and coworkers proposed the only other protocol for fundus-controlled dark adaptometry.[27,28] However, due to limitations of the MP1 microperimeter, their protocol necessitated adding filters to the optical path and changing the stimulus size during the examination to compensate for the low dynamic range. In addition, each test run had to be initiated manually, and no inter-device validation or retest reliability data were published for their method.[27] To overcome these limitations, we developed a new method based on the S-MAIA device.

We selected as hardware the widely available S-MAIA microperimetry device, which is widely distributed due to large multicenter studies such as MACUSTAR.[39] Because the device can be operated through OPI,[31,32] a graphical user interface through a web application could be developed using *R Shiny*.[33] The dark adaptation application is now available for non-technical users and provides flexibility regarding the testing grid and stimulus color (i.e. cyan and red testing versus only cyan testing).

As a critical prerequisite for the clinical application, this study established the concurrent validity, retest reliability, and construct validity of the devised method. The dynamic dark adaptation metrics (cone-rod break, RIT, and S2 slope) were concordant among the comparator and the devised method. Importantly, the minor between-device biases of these metrics were markedly smaller than the retest variability,[40] and typical disease-associated changes.[11]

The steady-state cone thresholds were – accounting for the instrument-specific difference in the dB-scale – in agreement as indicated by the tight limits of agreement. Interestingly, the absolute differences for the cone minus rod thresholds were larger in MonCvONE- than in S-MAIA-based measurements (e.g. at 6 degrees 2.3 vs. 1.8 LogUnits, cf., Supplementary Table S2). This difference is most likely attributable to two stimulus size-related factors: first, the fundus-controlled Goldmann III stimuli (diameter of 0.43 degrees or 125 µm) will stimulate to a lesser degree, rod photoreceptors distant to the locus center compared to Goldmann V stimuli (diameter of 1.72 degrees or 500 µm). This can affect rod thresholds given that all loci were within the region where rod photoreceptor density increases steeply with eccentricity.[41] Second, the perception of the Goldmann III stimulus is most likely affected by a shifting of the spatial summation curves during dark adaptation. Whereas the Goldmann V stimulus exceeds Ricco's area in photopic and scotopic spatial summation curves (in the central macula), the Goldmann III stimulus exceeds Ricco's area under photopic conditions, but not under scotopic conditions.[42–45] Thus, the S-MAIA-based cone thresholds are measured with complete or near complete spatial summation, whereas rod thresholds are measured along the ascending arm of the intensity-response function.

The retest reliability estimates were similar to previously reported data for all dark adaptation curve parameters, underscoring the devised method's relia-

bility.[40] Importantly, there was no evidence of a learning effect. This is likely attributable to the nature of dark adaptometry with repeated testing. For example, the cone thresholds were typically based on four or more threshold determinations, and even more threshold determinations were part of the S2 slope and rod threshold. Thus, variability in individual threshold determinations has little effect on the parameters determined by curve fitting.

Our cone and rod thresholds match the photoreceptor distribution (i.e. lowest cone threshold at 2 degrees, and lowest final rod threshold at 6 degrees).[41] The steeper age-associated decline of rod-related function is compatible with histopathologic studies documenting severe age-associated rod loss between 0.5 and 3 mm eccentricity.[30] In addition, our estimates for the cone-rod break and RIT at 4 degrees and 6 degrees are – when accounting for age differences (cf., effect of age estimate in Supplementary Table S5) – similar to previous data in healthy adults and patients with early AMD that used 50% to 70% rhodopsin bleaches.[14,46,47]

Limitations

Our study was restricted to healthy volunteers, so it is yet to be determined how effective our methods will be in patients with retinal diseases. We hypothesize that fundus-controlled dark adaptometry will provide even greater benefits over free-viewing dark adaptometry in patients with suboptimal or unstable fixation. Our study was only powered to uncover a clinically relevant between-device bias for the RIT of >1 minute (based on the difference between healthy volunteers and patients with intermediate AMD).[11] A markedly larger sample size is necessary to obtain normative data with age-dependent centile curves for each parameter.

In summary, we devised a novel method for fundus-controlled dark adaptometry. Key advantages of the devised method are the wide availability of the microperimetry device, the ability to perform dark adaptometry in patients with unstable fixation, and the flexibility of the developed software enabling custom tests. Fundus-controlled dark adaptometry will facilitate monitoring localized changes in rod function in clinical trials for IRDs and AMD.

Acknowledgments

Funded by a grant of the foundation: Pro sanandis oculis, Stiftung der Basler Kantonalbank zu Gunsten des Augenspitals in Basel (awarded to M.P.), and by a Retina Suisse doctoral thesis grant (awarded to J.O.).

Disclosure: **J.M. Oertli**, None; **K. Pfau**, Daiichi Sankyo (C); **H.P.N. Scholl**, Swiss National Science Foundation (#310030_201165) (F), the Wellcome Trust (PINNACLE study) (F), and the Foundation Fighting Blindness Clinical Research Institute (ProgStar study) (F), Astellas Pharma Global Development, Inc./Astellas Institute for Regenerative Medicine (S), Boehringer Ingelheim Pharma GmbH & Co (S), Gyroscope Therapeutics Ltd. (S), Janssen Research & Development, LLC (Johnson & Johnson) (S), Novartis Pharma AG (CORE) (S), Okuvision GmbH (S), and Third Rock Ventures, LLC (S), Gerson Lehrman Group (C), Guidepoint Global, LLC (C), and Tenpoint Therapeutics Limited (C), Data Monitoring and Safety Board/Committee of Belite Bio (CT2019-CTN-04690-1), ReNeuron Group Plc/Ora Inc. (NCT02464436), F. Hoffmann-La Roche Ltd (VELODROME trial, NCT04657289; DIAGRID trial, NCT05126966), and member of the Steering Committee of Novo Nordisk (FOCUS trial; NCT03811561) (N); **B.G. Jeffrey**, None; **M. Pfau**, Novartis (R), Janssen Pharmaceutica (C), Apellis (F, C)

References

1. Cideciyan AV, Pugh ENJ, Lamb TD, Huang Y, Jacobson SG. Rod plateaux during dark adaptation in Sorsby's fundus dystrophy and vitamin a deficiency. *Invest Ophthalmol Vis Sci*. 1997;38(9):1786–1794.
2. Steinmetz RL, Polkinghorne PC, Fitzke FW, Kemp CM, Bird AC. Abnormal dark adaptation and rhodopsin kinetics in Sorsby's fundus dystrophy. *Invest Ophthalmol Vis Sci*. 1992;33(5):1633–1636.
3. Jacobson SG, Cideciyan AV, Regunath G, et al. Night blindness in Sorsby's fundus dystrophy reversed by vitamin A. *Nat Genet*. 1995;11(1):27–32.
4. Jacobson SG, Cideciyan A V, Wright E, Wright AF. Phenotypic marker for early disease detection in dominant late-onset retinal degeneration. *Invest Ophthalmol Vis Sci*. 2001;42(8):1882–1890.
5. Hess K, Gliem M, Birtel J, et al. Impaired dark adaptation associated with a diseased Bruch membrane in pseudoxanthoma elasticum. *Retina*. 2020;40(10):1988–1995.
6. Raming K, Gliem M, Charbel Issa P, et al. Visual dysfunction and structural correlates in

Sorsby fundus dystrophy. *Am J Ophthalmol*. 2022;234:274–284.
7. Cideciyan AV, Haeseleer F, Fariss RN, et al. Rod and cone visual cycle consequences of a null mutation in the 11-cis-retinol dehydrogenase gene in man. *Vis Neurosci*. 2000;17(5):667–678.
8. Cideciyan AV, Aleman TS, Boye SL, et al. Human gene therapy for RPE65 isomerase deficiency activates the retinoid cycle of vision but with slow rod kinetics. *Proc Natl Acad Sci USA*. 2008;105(39):15112–15117.
9. Steinmetz RL, Haimovici R, Jubb C, Fitzke FW, Bird AC. Symptomatic abnormalities of dark adaptation in patients with age-related Bruch's membrane change. *Br J Ophthalmol*. 1993;77(9):549–554.
10. Owsley C, McGwin G, Jackson GR, et al. Effect of short-term, high-dose retinol on dark adaptation in aging and early age-related maculopathy. *Invest Ophthalmol Vis Sci*. 2006;47(4):1310–1318.
11. Hess K, de Silva T, Grisso P, et al. Evaluation of cone- and rod-mediated parameters in dark adaptation testing as outcome measures in age-related macular degeneration. *Ophthalmol Retin*. 2022;6(12):1173–1184.
12. Nigalye AK, Hess K, Pundlik SJ, Jeffrey BG, Cukras CA, Husain D. Dark adaptation and its role in age-related macular degeneration. *J Clin Med*. 2022;11(5):1358.
13. Fleckenstein M, Keenan TDL, Guymer RH, et al. Age-related macular degeneration. *Nat Rev Dis Prim*. 2021;7(1):31.
14. Flynn OJ, Cukras CA, Jeffrey BG. Characterization of rod function phenotypes across a range of age-related macular degeneration severities and subretinal Drusenoid deposits. *Invest Ophthalmol Vis Sci*. 2018;59(6):2411–2421.
15. Curcio CA, Owsley C, Jackson GR. Spare the rods, save the cones in aging and age-related maculopathy. *Investig Ophthalmol Vis Sci*. 2000;41(8):2015–2018.
16. Jacobson SG, Voigt WJ, Parel JM, et al. Automated light- and dark- adapted perimetry for evaluating retinitis pigmentosa. *Ophthalmology*. 1986;93(12):1604–1611.
17. McGuigan DB, Roman AJ, Cideciyan A V., et al. Automated light- and dark-adapted perimetry for evaluating retinitis pigmentosa: filling a need to accommodate multicenter clinical trials. *Invest Ophthalmol Vis Sci*. 2016;57(7):3118–3128.
18. Kelbsch C, Stingl K, Kempf M, et al. Objective measurement of local rod and cone function using gaze-controlled chromatic pupil campimetry in healthy subjects. *Transl Vis Sci Technol*. 2019;8(6):19.
19. Pfau M, Jolly JK, Wu Z, et al. Fundus-controlled perimetry (microperimetry): application as outcome measure in clinical trials. *Prog Retin Eye Res*. 2021;82:100907, https://doi.org/10.1016/j.preteyeres.2020.100907.
20. Crossland MD, Luong VA, Rubin GS, Fitzke FW. Retinal specific measurement of dark-adapted visual function: validation of a modified microperimeter. *BMC Ophthalmol*. 2011;11(1):5.
21. Pfau M, Lindner M, Müller PL, et al. Effective dynamic range and retest reliability of dark-adapted two-color fundus-controlled perimetry in patients with macular diseases. *Invest Ophthalmol Vis Sci*. 2017;58(6):BIO158–BIO167.
22. von der Emde L, Pfau M, Thiele S, et al. Mesopic and dark-adapted two-color fundus-controlled perimetry in choroidal neovascularization secondary to age-related macular degeneration. *Transl Vis Sci Technol*. 2019;8(1):7.
23. Krishnan AK, Roman AJ, Swider M, Jacobson SG, Cideciyan AV. Macular Rod function in retinitis pigmentosa measured with scotopic microperimetry. *Transl Vis Sci Technol*. 2021;10(11):3.
24. Jolly JK, Nanda A, Buckley TMW, Pfau M, Bridge H, MacLaren RE. Assessment of scotopic function in rod–cone inherited retinal degeneration with the scotopic macular integrity assessment. *Transl Vis Sci Technol*. 2023;12(2):10.
25. Jackson GR, Scott IU, Kim IK, Quillen DA, Iannaccone A, Edwards JG. Diagnostic sensitivity and specificity of dark adaptometry for detection of age-related macular degeneration. *Invest Ophthalmol Vis Sci*. 2014;55(3):1427–1431.
26. Owsley C, Swain TA, McGwin GJ, Clark ME, Kar D, Curcio CA. Biologically guided optimization of test target location for rod-mediated dark adaptation in age-related macular degeneration: alabama study on early age-related macular degeneration 2 baseline. *Ophthalmol Sci*. 2023;3(2):100274.
27. Bowl W, Stieger K, Lorenz B. Fundus-controlled two-color dark adaptometry with the microperimeter MP1. *Graefe's Arch Clin Exp Ophthalmol*. 2015;253(6):965–972.
28. Bowl W, Lorenz B, Stieger K, Schweinfurth S, Holve K, Andrassi-Darida M. Fundus-controlled dark adaptometry in young children without and with spontaneously regressed retinopathy of prematurity. *Transl Vis Sci Technol*. 2019;8(3):62.
29. Thomas MM, Lamb TD. Light adaptation and dark adaptation of human rod photoreceptors

measured from the a-wave of the electroretinogram. *J Physiol*. 1999;518(Pt 2):479–496.
30. Curcio CA, Allen KA. Aging of the human photoreceptor mosaic: evidence for selective vulnerability of rods in central retina. *Invest Ophthalmol Vis Sci*. 1993;34(12):3278–3296.
31. Turpin A, Artes PH, McKendrick AM. The open perimetry interface: an enabling tool for clinical visual psychophysics. *J Vis*. 2012;12(11):22, https://doi.org/10.1167/12.11.22.
32. Turpin A. OPI: open perimetry interface. 2022. Available at: https://cran.r-project.org/package=OPI.
33. Chang W, Cheng J, Allaire JJ, et al. shiny: web application framework for R. 2022. Available at: https://cran.r-project.org/package=shiny.
34. Bürkner P-C. brms: an R package for Bayesian multilevel models using Stan. *J Stat Softw*. 2017;80(1):1–28.
35. Jackson GR, Owsley C, McGwin G. Aging and dark adaptation. *Vision Res*. 1999;39(23):3975–3982.
36. Pfau M, Müller PL, Von Der Emde L, et al. Mesopic and dark-adapted two-color fundus-controlled perimetry in geographic atrophy secondary to age-related macular degeneration. *Retina*. 2020;40(1):169–180.
37. Pfau M, von der Emde L, Dysli C, et al. Light sensitivity within areas of geographic atrophy secondary to age-related macular degeneration. *Invest Ophthalmol Vis Sci*. 2019;60(12):3992–4001.
38. Pfau M, von der Emde L, Dysli C, et al. Determinants of cone- and rod-function in geographic atrophy: AI-based structure-function correlation. *Am J Ophthalmol*. 2020;217:162–173.
39. Terheyden JH, Holz FG, Schmitz-Valckenberg S, et al. Clinical study protocol for a low-interventional study in intermediate age-related macular degeneration developing novel clinical endpoints for interventional clinical trials with a regulatory and patient access intention-MACUSTAR. *Trials*. 2020;21(1):659.
40. Uddin D, Jeffrey BG, Flynn O, et al. Repeatability of scotopic sensitivity and dark adaptation using a Medmont dark-adapted chromatic perimeter in age-related macular degeneration. *Transl Vis Sci Technol*. 2020;9(7):31.
41. Curcio CA, Sloan KR, Kalina RE, Hendrickson AE. Human photoreceptor topography. *J Comp Neurol*. 1990;292(4):497–523.
42. Montesano G, Mulholland PJ, Garway-Heath DF, Evans J, Ometto G, Crabb DP. Spatiotemporal summation of perimetric stimuli in healthy observers. *J Vis*. 2023;23(4):2.
43. Hansen RM, Hamer RD, Fulton AB. The effect of light adaptation on scotopic spatial summation in 10-week-old infants. *Vision Res*. 1992;32(2):387–392.
44. Lelkens AM, Zuidema P. Increment thresholds with various low background intensities at different locations in the peripheral retina. *J Opt Soc Am*. 1983;73(10):1372–1378.
45. Schefrin BE, Bieber ML, McLean R, Werner JS. The area of complete scotopic spatial summation enlarges with age. *J Opt Soc Am A Opt Image Sci Vis*. 1998;15(2):340–348.
46. Tahir HJ, Rodrigo-Diaz E, Parry NRA, et al. Slowed dark adaptation in early AMD: dual stimulus reveals scotopic and photopic abnormalities. *Invest Ophthalmol Vis Sci*. 2018;59(4):AMD202–AMD210.
47. Jeffrey BG, Flynn OJ, Huryn LA, Pfau M, Cukras CA. Scotopic contour deformation detection reveals early rod dysfunction in age-related macular degeneration with and without reticular pseudodrusen. *Invest Ophthalmol Vis Sci*. 2022;63(6):23.